



OPEN

Intracellular oxygen metabolism during bovine oocyte and preimplantation embryo development

Paul J. McKeegan^{1,2}, Selina F. Boardman^{1,3}, Amy A. Wanless^{1,4}, Grace Boyd^{1,5}, Laura J. Warwick^{1,6}, Jianping Lu¹, Keerthi Gnanaprabha^{1,7} & Helen M. Picton¹

We report a novel method to profile intracellular oxygen concentration (icO₂) during in vitro mammalian oocyte and preimplantation embryo development using a commercially available multimodal phosphorescent nanosensor (MM2). Abattoir-derived bovine oocytes and embryos were incubated with MM2 in vitro. A series of inhibitors were applied during live-cell multiphoton imaging to record changes in icO₂ associated with mitochondrial processes. The uncoupler carbonyl cyanide-p-trifluoromethoxyphenylhydrazone (FCCP) uncouples mitochondrial oxygen consumption to its maximum, while antimycin inhibits complex III to ablate mitochondrial oxygen consumption. Increasing oxygen consumption was expected to reduce icO₂ and decreasing oxygen consumption to increase icO₂. Use of these inhibitors quantifies how much oxygen is consumed at basal in comparison to the upper and lower limits of mitochondrial function. icO₂ measurements were compared to mitochondrial DNA copy number analysed by qPCR. Antimycin treatment increased icO₂ for all stages tested, suggesting significant mitochondrial oxygen consumption at basal. icO₂ of oocytes and preimplantation embryos were unaffected by FCCP treatment. Inner cell mass icO₂ was lower than trophectoderm, perhaps reflecting limitations of diffusion. Mitochondrial DNA copy numbers were similar between stages in the range 0.9–4 × 10⁶ copies and did not correlate with icO₂. These results validate the MM2 probe as a sensitive, non-toxic probe of intracellular oxygen concentration in mammalian oocytes and preimplantation embryos.

Abbreviations

icO ₂	Intracellular oxygen concentration
EGA	Embryonic genome activation
MM2	Pt(II)-5,10,15,20-tetrakis-(2,3,4,5,6-pentafluorophenyl)-porphyrin and poly(9,9-dioctylfluorene) intracellular probe
PtTFPP	Pt(II)-5,10,15,20-tetrakis-(2,3,4,5,6-pentafluorophenyl)-porphyrin
PFO	Poly(9,9-dioctylfluorene)
PBS	Phosphate buffered saline
HEPES	4-(2-Hydroxyethyl)-1-piperazineethanesulfonic acid
BSA	Bovine serum albumin
BSA-FAF	Bovine serum albumin—fatty acid free
FSH	Follicle stimulating hormone
LH	Luteinising hormone
IVM	In vitro maturation
IVF	In vitro fertilisation

¹Reproduction and Early Development Research Group, Leeds Institute of Cardiovascular and Metabolic Medicine, School of Medicine, University of Leeds, Clarendon Way, Leeds LS2 9JT, UK. ²Centre for Anatomical and Human Sciences, Hull York Medical School, University of Hull, Hull HU6 7RX, UK. ³CARE Fertility, Manchester, England, UK. ⁴Assisted Conception Unit, Ninewells Hospital, Dundee, Scotland, UK. ⁵Department of Biological Sciences, University of York, Wentworth Way, York YO10 5DD, England, UK. ⁶St James's University Hospital, Beckett Street, Leeds LS9 7TF, England, UK. ⁷GCRM Fertility, 21 Fifty Pitches Way, Glasgow G51 4FD, Scotland, UK. ✉email: paul.mckeegan@hyms.ac.uk

IVP	In vitro production
COC	Cumulus-oocyte complex
MEM	Minimum essential medium
M199	Medium 199
TALP	Tyrode's albumin lactate pyruvate medium
HM	Holding medium
SOF	Synthetic oviduct fluid
LSM	Laser scanning microscope
FCCP	Carbonyl cyanide-p-trifluoromethoxyphenylhydrazone
mtDNA	Mitochondrial deoxyribonucleic acid
PCR	Polymerase chain reaction
qPCR	Quantitative real-time polymerase chain reaction
COI	Cytochrome c oxidase subunit 1
ICM	Inner cell mass
TE	Trophectoderm
PI	Propidium iodide
ANOVA	Analysis of variance
ATP	Adenosine triphosphate
OXPPOS	Oxidative phosphorylation
AA	Antimycin A

Regulated mitochondrial function is responsible for energy-releasing metabolic reactions, cell signalling and apoptosis and is vital to the developing embryo. Mitochondrial dysfunction may lead to developmental arrest, embryo death or developmental failure *in utero*^{1–3}, and has been implicated in the development of a range of diseases in childhood or adulthood, such as autism^{4,5} and Alzheimer's^{6–8}. Furthermore, studies suggest that mitochondrial DNA content may predict embryo viability in assisted reproduction therapies⁹. More detailed understanding of mitochondrial function in oocytes and developing embryos is however needed to improve our understanding of how early development affects health and disease throughout life.

Oxidative phosphorylation. The primary function of mitochondria is to provide energy in the form of Adenosine Triphosphate (ATP) which is coupled to the consumption of oxygen by oxidative phosphorylation (OXPPOS)¹⁰. Therefore, ATP synthesis and oxygen consumption are tightly linked and regulated. Whilst glycolytic activity also produces ATP in oocytes and early embryos, dramatically more ATP is produced by OXPPOS^{11–13}. Oxygen consumption therefore directly correlates to levels of aerobic respiration and is used as a marker of overall metabolism in mammalian oocytes and embryos^{12,14} which may reflect embryo viability¹⁵. OXPPOS reportedly increases during preimplantation embryo development to provide an increasing proportion of total ATP in order to meet the increasing energy demand of protein synthesis and blastocoel formation^{15,16}. Additionally, by the blastocyst stage, cells have differentiated into trophoctoderm (TE), from which placenta tissue is derived, and inner cell mass (ICM), which gives rise to the fetus. These cell types are believed to have different metabolic phenotypes¹⁷, with TE notably more metabolically active than ICM. However, there is currently no established method to measure TE vs ICM metabolism without biopsy.

Measuring oxygen metabolism. Due to the vital role of oxygen in mitochondrial metabolism, several methods of measuring oxygen consumption in the oocyte and embryo have been reported. Contemporary and emerging methods include the Unisense Nano respirometer^{15,18}, the self-referencing electrode¹⁹ and bespoke electrochemical devices^{20,21}. Recent developments include combining electrochemistry with microfluidic technologies^{22,23} for embryo-compatible devices. Obeidat and colleagues²⁴ report detecting oxygen consumption alongside glucose consumption, lactate production and pH in individual equine blastocysts using multiple electrochemical sensors. Extracellular flux analysis using the Seahorse Bioanalyzer (Agilent) has recently been published as a more user-friendly, rapid method of profiling the components of respiration in small groups of oocytes or preimplantation embryos²⁵. However there has to date been no report of changes in intracellular oxygen concentration (icO₂) within the oocyte or embryo itself.

Probing mitochondrial function. As noted previously, coupling of mitochondrial oxygen consumption to ATP production is tightly regulated within tissues. However, it is notable that tissues can modulate mitochondrial oxygen consumption and ATP production to fulfil other roles, such as heat generation by brown adipose tissue^{27,28}. And that the contributions of different mitochondrial complexes and processes can be elucidated using metabolic poisons, as recently reported by the Sturmey group^{25,29}. Exogenous uncouplers, such as carbonyl cyanide-p-trifluoromethoxyphenylhydrazone (FCCP), disrupt the regulation of the proton gradient and increase mitochondrial oxygen consumption to its maximum, whilst preventing production of ATP by OXPPOS^{14,25,28–30}. FCCP also leads to reduced ATP content in human oocytes³¹, as well as increased glucose consumption and a shift in redox state in equine embryos³¹. The difference between basal and maximal oxygen consumption reveals the spare respiratory capacity; a phenomenon which can enable tissues to adapt to changing ATP demand³⁰. Inhibitors of mitochondrial protein complex III, such as antimycin, block mitochondrial oxygen consumption and mitochondrial ATP production completely^{14,25,28–30}. These are used to quantify the contributions of mitochondrial and non-mitochondrial oxygen consumption *in vitro*.

Embryo mitochondria. It is an essential requirement that the number, localisation and function of mitochondria are sufficient to support oocyte developmental competence through OXPPOS^{3,26,32}. Indeed, oocyte maturation reportedly involves a burst of mitochondrial DNA replication, as indicated by mitochondrial DNA copy number^{33,34}.

However, the number of mitochondria per embryo remain fixed from the 1 cell zygote to the 100–200 cell blastocyst, as the cellular machinery necessary to replicate the organelles are not present until postimplantation^{26,36,37}. Mitochondria mature from a globular, condensed form into the elongated classical structure with an increased number of cristae during preimplantation development²⁶. This occurs in parallel with an increase in OXPPOS activity from the zygote to the blastocyst^{52,66,67}. It is tempting to speculate that the resulting increase in surface area:volume ratio could increase mitochondrial function without changing the number of mitochondria. This study therefore aims to investigate whether sensitivity of icO₂ to maximal and ablated mitochondrial oxygen consumption, indicated by FCCP and antimycin respectively, change during in vitro oocyte maturation and preimplantation embryo development in line with mitochondrial maturation.

The MM2 icO₂ probe. One reported method to measure icO₂ in mammalian cell culture is the multimodal MM2 probe, developed by Papkovsky and colleagues³⁸. Several studies report that this and similar nanoparticle probes are suitable for highly sensitive ratiometric measurements in a variety of tissue types including monolayer and spheroid cultures^{38–42}. MM2 is an intracellular label consisting of an oxygen-sensitive phosphorescent reporter dye Pt(II)-5,10,15,20-tetrakis-(2,3,4,5,6-pentafluorophenyl)-porphyrin (PtTFPP; emission at 650 nm) and a poly(9,9-dioctylfluorene) reference fluorophore (PFO, emission at 410–450 nm), within 70 nm nanoparticles³⁸. The probe is ratiometric; the PtTFPP emission peak at 650 nm is quenched by oxygen, while the PFO emission peak at 440 nm is oxygen insensitive and hence used as a loading control. Quantification is possible using a simple 2-point calibration curve comprised of an aqueous solution in atmospheric conditions (21%, normoxic), and a second fixed sample with a chemical oxygen scavenger to remove all oxygen from the surrounding solution (0%, anoxic)⁴⁰. Samples must be fixed to eliminate any effect of oxygen consuming activity. This 2-point calibration approach is widely used in the literature, including by the Papkovsky group, who developed the suite of probes including MM2 and corresponding protocols⁴⁰, but also across a wide variety of fluorescence^{43–46} and electrode-based^{18,45–48} methods to profile oxygen metabolism. To the authors' knowledge this is the first example of the use of the MM2 probe in mammalian oocyte and embryo tissue.

The aim of this work was to develop a new method to visualise icO₂ in abattoir-derived individual oocytes and embryos in vitro, allowing resolution of different regions within the oocyte or embryo and identification of zones of high and low metabolic activity. We first optimised incubation conditions (Fig. 1) and verified whether cumulus cell layers were necessary for oocyte labelling (Fig. 2). We then used FCCP and antimycin to profile icO₂ within the limits of mitochondrial control in oocytes and preimplantation embryos (Fig. 3). We then report use of the MM2 probe to quantify icO₂ in ICM and TE regions of blastocysts (Fig. 4), correlation of icO₂ to blastocyst cell count and cell allocation to ICM and TE lineages (Fig. 5) and finally correlation to mtDNA copy number (Fig. 6).

Results

Validation and optimisation of the MM2 probe in oocytes and embryos. Incubation times of between 3 and 24 h have been reported for loading the MM2 probe^{38,49,50}. Groups of in vitro derived day 7 bovine blastocysts were incubated for 3, 6, 18 or 24 h with 10 µg/ml MM2 probe in SOFaaBSA before multiphoton imaging (n = 6 per group, total n = 24). The mean signal ratio did not differ statistically dependent on incubation time and ranged from 0.10 ± 0.01 IU to 0.25 ± 0.1 IU (p = 0.84, Fig. 1A). However, variation was lowest at the 24 h time point. Therefore, 24 h incubation time was selected for reproducibility and ease of use.

Next, blastocysts were labelled and imaged with 1 µg/ml, 5 µg/ml or 10 µg/ml MM2 probe in SOFaaBSA over 24 h (n = 6 per group, 3 independent groups). The mean signal ratio ranged from 0.24 ± 0.04 IU to 0.4 ± 0.02 IU (Fig. 1B). No significant difference in signal was found between the 3 different concentrations used (p = 0.8). An incubation concentration of 5 µg/ml MM2 was selected for all remaining experiments in line with loading concentrations previously reported by the Papkovsky group^{42,50}.

2-Point calibration of MM2 signal with the corresponding sample of interest was performed in order to calculate icO₂. An example blastocyst calibration curve is shown in (Fig. 1C). The mean signal ratio of fixed MM2-stained blastocysts under anoxia (0% O₂) was 0.84 ± 0.002 (n = 3). This was significantly higher (p < 0.0001) than the mean signal ratio of fixed blastocysts labelled and imaged under normoxia (21% O₂) (0.10 ± 0.04, n = 3), producing a calibration curve with the equation $y = -0.0035x + 0.84$.

The effect of cumulus cells on MM2 labelling efficacy and oxygen concentration. Oocytes were randomly assigned into denuded or intact cumulus-enclosed groups and labelled with 5 µg/ml MM2 for 3 h (Fig. 2). Denuded oocyte icO₂ (129.50 ± 18.07 µmol/l, n = 29) reduced significantly following FCCP treatment (99.13 ± 20.14 µmol/l, p < 0.0001) and returned to an intermediate level following antimycin exposure (119.7 ± 13.20 µmol/l, p > 0.05, Fig. 2). Cumulus-enclosed oocyte icO₂ (121.60 ± 13.15 µmol/l, n = 28) reduced significantly following FCCP treatment (98.60 ± 10.21 µmol/l, p < 0.0001) and significantly increased following antimycin exposure (126.00 ± 4.40 µmol/l, p < 0.005, Fig. 2). The presence or absence of cumulus cells did not have any significant effect on the MM2 signal or icO₂ (p > 0.05).

icO₂ throughout in vitro oocyte maturation and embryo development. *Oocytes.* Immature oocyte icO₂ (94.76 ± 27.28 µmol/l, n = 21) reduced significantly following FCCP treatment (93.39 ± 24.06 µmol/l, p < 0.005) and significantly increased following antimycin exposure (116.6 ± 43.59 µmol/l, p < 0.005, Fig. 3A).

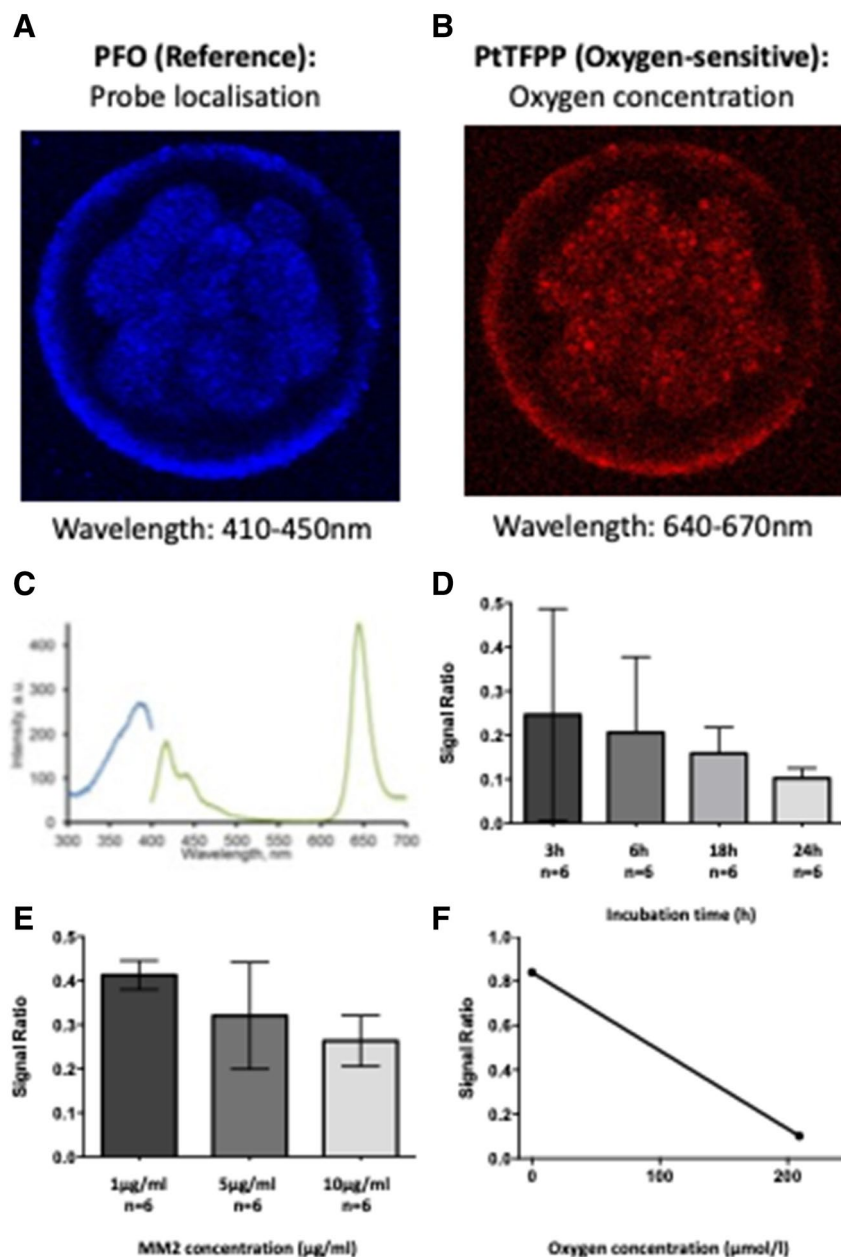


Figure 1. Optimisation and calibration of MM2 incubation conditions. Examples images (A) PFO oxygen-insensitive fluorophore labelling; (B) PtTFPP oxygen-sensitive labelling; (C) Excitation/Emission spectra reproduced from manufacturer guidance; (D) Signal ratio comparison following blastocyst incubation with MM2 probe for 3 (n=6), 6 (n=6), 18 (n=6) and 24 h (n=6), with no statistical differences; (E) Blastocysts imaged after 24 h incubation with 1 µg/ml (n=6), 5 µg/ml (n=6), or 10 µg/ml (n=6) MM2 probe with no significant differences; (F) Example calibration based on blastocysts imaged at 0% and 21% O₂ (p < 0.0001) with curve $y = -0.0035x + 0.84$. Values plotted as mean ± SD for the number of analyses shown.

Mature oocyte icO₂ (90.56 ± 18.73 µmol/l, n=16) was significantly reduced following FCCP treatment (92.97 ± 14.46 µmol/l, p < 0.0005) and increased significantly following antimycin exposure (122.1 ± 29.73 µmol/l, p < 0.005, Fig. 3B).

Embryos. Early cleavage stages were grouped into early cleavage (EC) stages (2–7 cell) and late cleavage (LC) stages (8–32 cell) for quantitative analysis. EC basal icO₂ (84.84 ± 34.37 µmol/l, n=23) was significantly reduced following FCCP treatment (80.78 ± 34.66 µmol/l, p < 0.0005). icO₂ increased following antimycin treatment (122.90 ± 28.60 µmol/l, p < 0.0005, Fig. 3C). LC basal icO₂ (110.1 ± 30.03 µmol/l, n=26) was similar to FCCP-treated icO₂ (93.73 ± 36.91 µmol/l, p > 0.05). However, following antimycin treatment (135.70 ± 34.14 µmol/l, Fig. 3D), icO₂ was significantly higher than basal (p < 0.05) and FCCP treatment (p < 0.0005). EC basal icO₂ was significantly lower than that of LC embryos (p < 0.05) and blastocysts (p < 0.005).

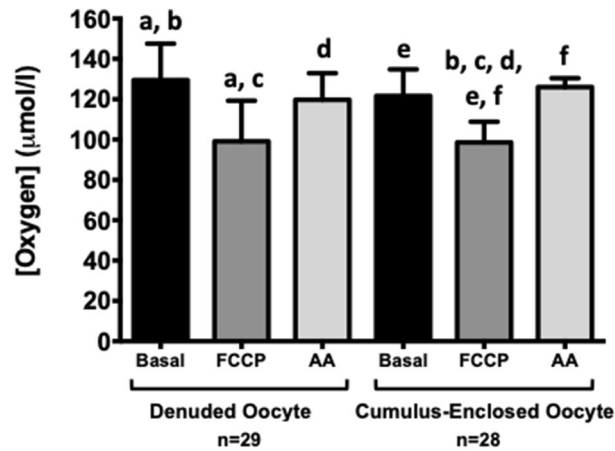


Figure 2. The effect of cumulus complex presence on oocyte oxygen concentration. Change in denuded oocyte icO_2 ($n=29$): Basal ($129.50 \pm 18.07 \mu\text{mol/l}$), FCCP treated ($99.13 \pm 20.14 \mu\text{mol/l}$, $p=0.0002$) and antimycin treated ($119.7 \pm 13.20 \mu\text{mol/l}$, $p>0.05$). Change in cumulus-enclosed oocyte icO_2 ($n=28$): Basal ($121.60 \pm 13.15 \mu\text{mol/l}$), FCCP treated ($98.60 \pm 10.20 \mu\text{mol/l}$, $p<0.0001$) and antimycin treated ($126.00 \pm 4.40 \mu\text{mol/l}$, $p<0.005$). Values plotted as mean \pm SD for the number of analyses shown. Values with the same letter indicate significant differences by ANOVA with post-hoc Tukey test.

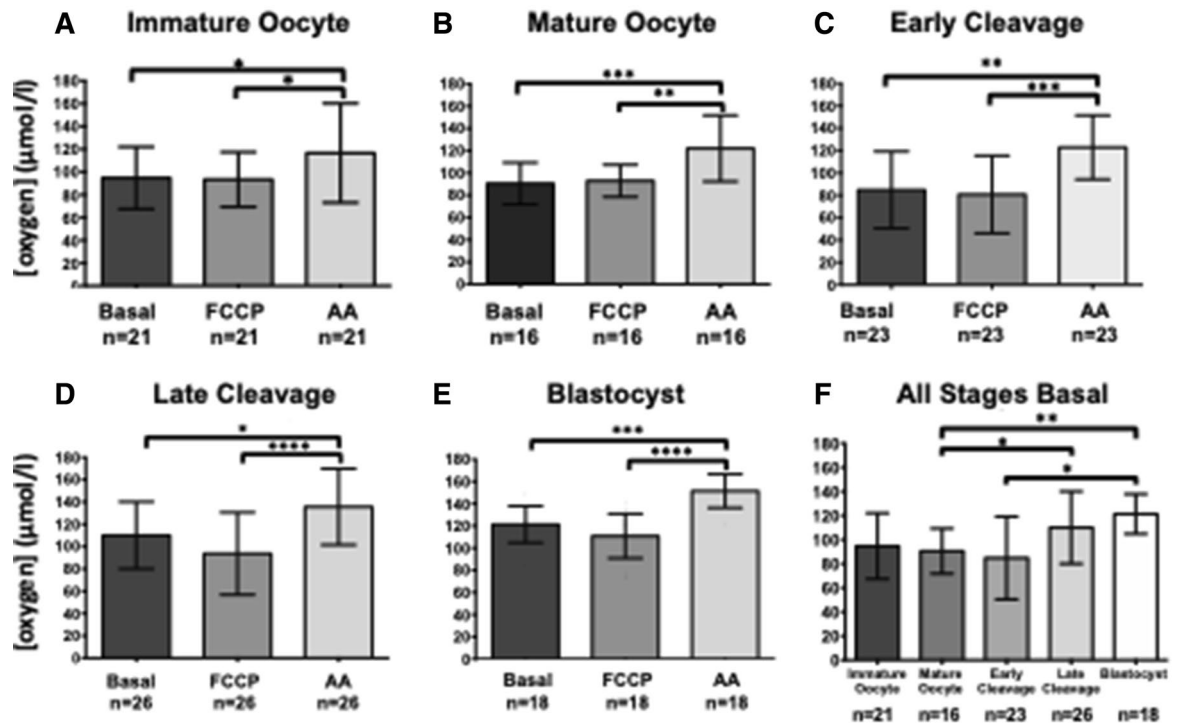


Figure 3. icO_2 throughout preimplantation development. Effect of FCCP and antimycin treatment on icO_2 of (A) immature oocytes ($n=21$) Basal ($94.76 \pm 27.28 \mu\text{mol/l}$), FCCP treated ($93.39 \pm 24.06 \mu\text{mol/l}$) and antimycin treated ($116.6 \pm 43.59 \mu\text{mol/l}$); (B) mature oocytes ($n=16$) Basal ($90.56 \pm 18.73 \mu\text{mol/l}$), FCCP treated ($92.97 \pm 14.46 \mu\text{mol/l}$) and antimycin treated ($122.1 \pm 29.73 \mu\text{mol/l}$); (C) EC embryos ($n=23$) Basal ($84.84 \pm 34.37 \mu\text{mol/l}$), FCCP treated ($80.78 \pm 34.66 \mu\text{mol/l}$) and antimycin treated ($122.90 \pm 28.60 \mu\text{mol/l}$); (D) LC embryos ($n=26$) Basal ($110.1 \pm 30.03 \mu\text{mol/l}$), FCCP treated ($93.73 \pm 36.91 \mu\text{mol/l}$) and antimycin treated ($135.70 \pm 34.14 \mu\text{mol/l}$); (E) Blastocysts ($n=18$) Basal ($121.4 \pm 16.51 \mu\text{mol/l}$), FCCP treated ($110.0 \pm 20.03 \mu\text{mol/l}$) and antimycin treated ($151.40 \pm 15.16 \mu\text{mol/l}$); (F) Basal icO_2 comparison between immature oocyte, mature oocyte, EC embryo, LC embryo and blastocyst stages. Values plotted as mean \pm SD for the number of analyses shown * $p<0.05$, ** $p<0.01$, *** $p<0.001$ and **** $p<0.0001$.

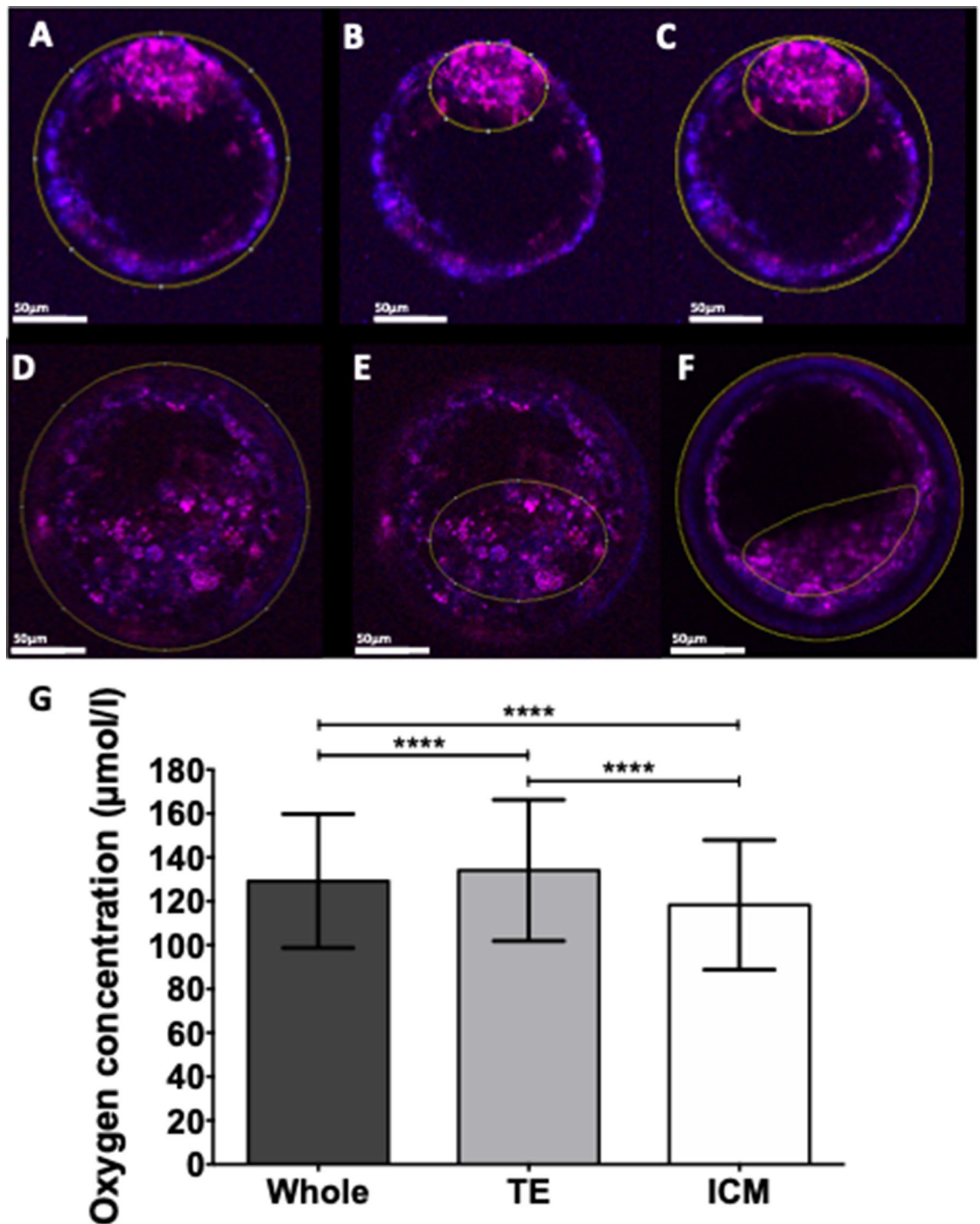


Figure 4. Blastocyst ICM and TE icO_2 . (A–F) Example of using ImageJ region of interest selection to measure relative signal intensity of (A, D) Whole blastocyst, (B, E) Inner Cell Mass (ICM) and (C, F) Trophectoderm (TE) regions. Merged images are shown; channels were measured individually. (G) Quantitative comparison of change in icO_2 between whole blastocyst ($129.23 \pm 30.54 \mu\text{mol/l}$), TE ($134.10 \pm 32.18 \mu\text{mol/l}$) and ICM ($118.33 \pm 29.57 \mu\text{mol/l}$, $n = 82$). Values plotted as mean \pm SD for the number of analyses shown **** $p < 0.0001$.

Blastocyst icO_2 decreased from basal levels ($121.4 \pm 16.51 \mu\text{mol/l}$, $n = 18$, Fig. 3E) following FCCP treatment ($110.0 \pm 20.03 \mu\text{mol/l}$, $p < 0.0005$) and increased with antimycin treatment ($151.40 \pm 15.16 \mu\text{mol/l}$, $p < 0.0001$).

Differences in basal oxygen concentration during oocyte maturation and embryo development. Basal icO_2 was similar between immature oocytes, mature oocytes, and EC embryos (Fig. 3F). icO_2 was increased in later stages,

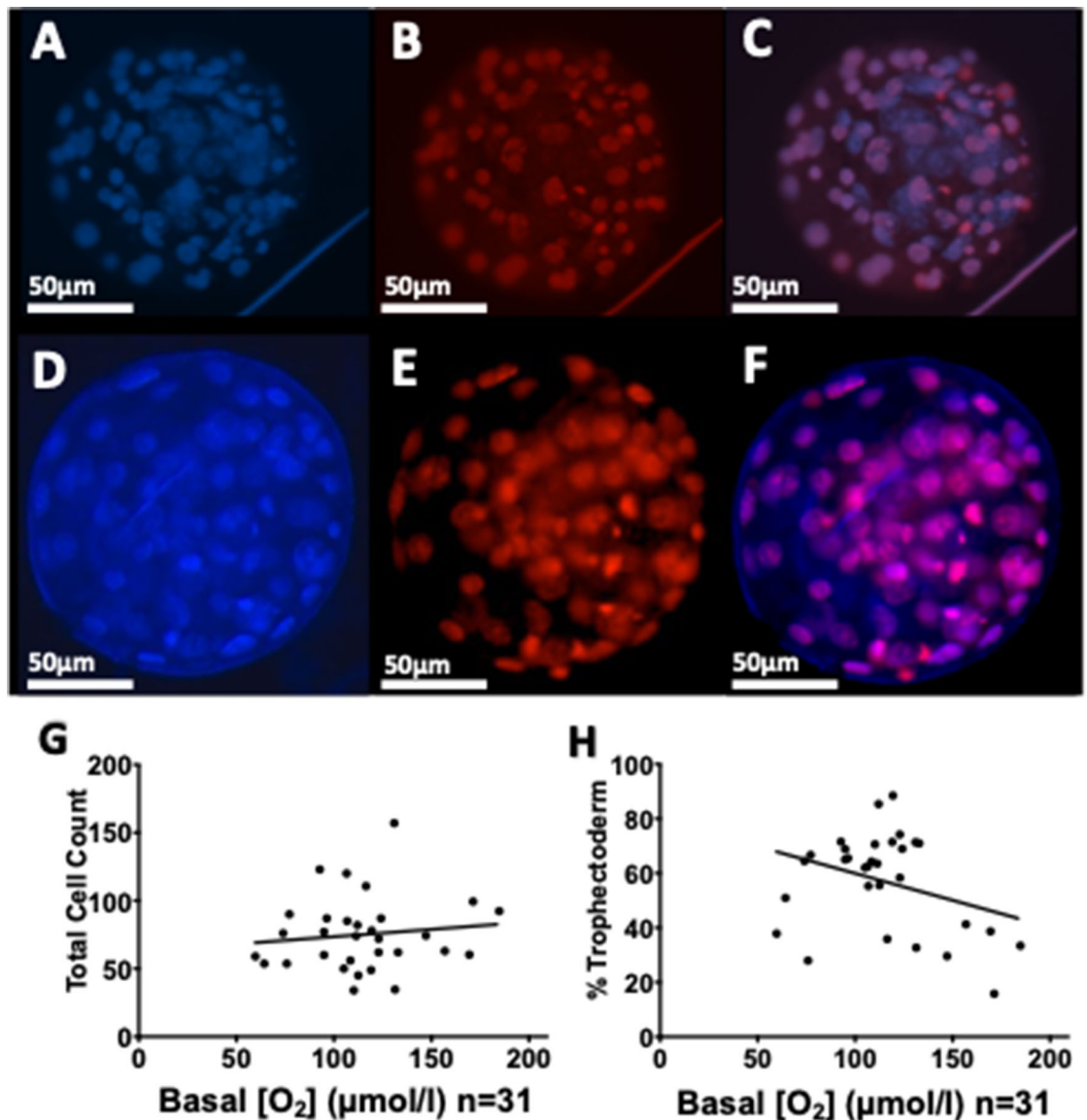


Figure 5. Blastocyst cell allocation and basal oxygen concentration. Examples shown of Hoechst total cell staining (A, D), Propidium Iodide (PI) Trophectoderm staining (B, E), combined channels (C, F). (G) Basal $i\text{cO}_2$ versus total cell count with line equation $y=0.1086x+62.62$, $R^2=0.015$, $p=0.52$. (H) Basal oxygen concentration versus % Trophectoderm with line equation $y=0.1974x+79.68$, $R^2=0.11$, $p=0.07$.

with LC embryo $i\text{cO}_2$ significantly higher than that of mature oocytes ($p < 0.05$) and blastocyst $i\text{cO}_2$ significantly higher than that of both mature oocytes ($p < 0.005$) and LC embryos ($p < 0.05$).

Blastocyst ICM and TE visual analysis. Blastocyst images were examined in ImageJ to compare MM2 signal intensity between whole blastocysts, ICM and TE regions (Fig. 4A–C). Mean overall blastocyst basal $i\text{cO}_2$ was 129.23 ± 30.54 $\mu\text{mol/l}$ ($n=82$, Fig. 4D). Trophectoderm (TE) oxygen concentration (134.10 ± 32.18 $\mu\text{mol/l}$) was significantly higher than ICM or overall ($p < 0.0001$). Inner Cell Mass (ICM) $i\text{cO}_2$ (118.33 ± 29.57 $\mu\text{mol/l}$) was significantly lower than either TE or overall ($p < 0.0001$).

Blastocyst cell allocation ratios. Blastocyst total cell counts (representative images: Fig. 5A–F) varied from 34 to 157 cells and were not normally distributed ($n=31$; $p=0.01$). Blastocyst cell allocation ratio (% TE) varied from 16 to 88% and were normally distributed ($n=31$; $p=0.35$). Neither total cell count ($75 \pm 4.8\%$; $p=0.07$; Fig. 5G), nor cell allocation ($57 \pm 3.2\%$; $p=0.52$; Fig. 5H) correlated with $i\text{cO}_2$.

Mitochondrial DNA. Mean MtDNA copy number was $1.75 \times 10^5 \pm 1.3 \times 10^4$ copies ($n=45$). There was no detected correlation between $i\text{cO}_2$ and mtDNA copy number (Fig. 6A; $n=42$; $R^2=0.05$; $p=0.14$). mtDNA copy number did not vary significantly between immature oocytes ($1.8 \times 10^5 \pm 1.6 \times 10^4$ copies; $n=10$), mature oocytes

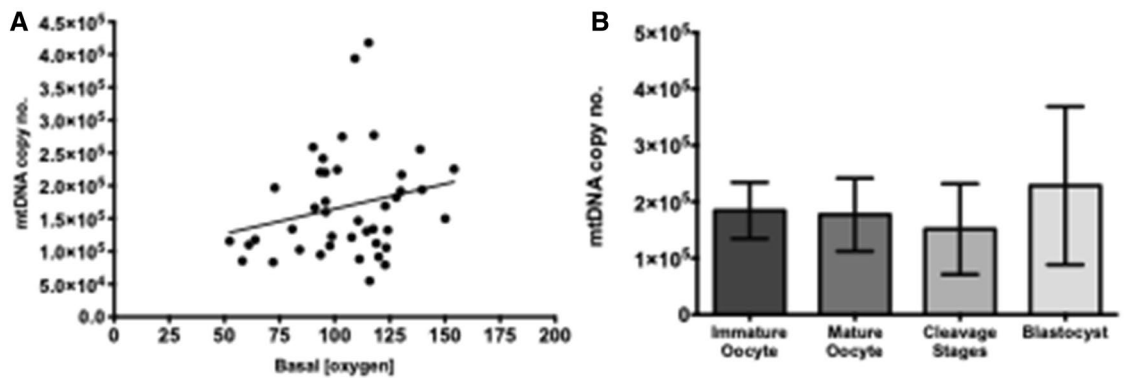


Figure 6. Mitochondrial DNA copy number. (A) Correlation of mtDNA copy number with basal oxygen level across all samples tested ($n = 42$) with line equation $y = 759.7x + 88,713$ ($R^2 = 0.05$, $p = 0.14$); (B) mtDNA copy number for immature oocytes ($1.75 \times 10^5 \pm 1.6 \times 10^4$ copies; $n = 10$), mature oocytes ($1.77 \times 10^5 \pm 2.6 \times 10^4$ copies; $n = 6$), cleavage stage embryos ($1.5 \times 10^5 \pm 1.8 \times 10^4$ copies; $n = 19$) and blastocysts ($2.3 \times 10^5 \pm 5.3 \times 10^4$ copies), with no significant differences. Data shown as mean \pm SD.

($1.77 \times 10^5 \pm 2.6 \times 10^4$ copies; $n = 6$), early cleavage stage embryos ($1.5 \times 10^5 \pm 1.8 \times 10^4$ copies; $n = 19$) or blastocyst ($2.3 \times 10^5 \pm 5.3 \times 10^4$ copies; $n = 7$; $p = 0.23$, Fig. 6B).

Discussion

We present a novel method to visualise and quantitatively assess icO_2 during oocyte maturation and preimplantation embryo development. Labelling with the MM2 probe was user-friendly and reproducible, with quantitation achieved using a simple 2-point calibration curve (Fig. 1). MM2 signal was sensitive to changes in mitochondrial oxygen metabolism and was used to profile icO_2 at basal, maximal (uncoupled) and non-mitochondrial levels of oxygen consumption using metabolic poisons (Figs. 2, 3). Furthermore, assessment of specific sample regions, namely blastocyst ICM and TE, has been achieved (Fig. 4). MM2 analysis has also been combined with blastocyst cell allocation ratio imaging and qPCR (Figs. 5, 6) and could be used in conjunction with other endpoint analyses.

Basal icO_2 was similar between immature and mature oocytes (Fig. 3A). The localisation of high MM2 signal intensity, indicating areas of low oxygen concentration, tended to be throughout the ooplasm of the immature oocyte and around the periphery of mature oocytes, comparable to the mitochondrial localisation reported by Sturmey et al.³²

To ascertain the effect of cumulus cells on oocyte MM2 loading efficiency and oxygen metabolism, COCs were randomly assigned to overnight culture in IVM media + 5 μ g/ml MM2 either with cumulus layers intact or following denudation. Cumulus presence did not affect icO_2 , with basal, FCCP and antimycin treated values similar between denuded and cumulus enclosed groups (Fig. 2). In both groups, FCCP significantly reduced icO_2 from basal levels, while antimycin returned oxygen concentration to basal levels. This suggests that (1) cumulus presence did not affect MM2 uptake or sensitivity to changes in oxygen level; and (2) MM2 was sensitive to changes in mitochondrially-regulated oxygen consumption in oocytes. Taken together, this suggests that MM2 is a suitable probe for use in oocytes with or without cumulus.

Oxygen concentration was profiled throughout oocyte maturation and preimplantation development. Basal icO_2 was highest in blastocysts, at a level significantly higher than in mature oocytes or early cleavage embryos (Fig. 3F). At each stage tested, FCCP treatment did not cause a significant decrease in icO_2 , however antimycin did cause a significant increase in icO_2 (Fig. 3A–E). Therefore, no significant changes in mitochondrial function during preimplantation development were detected. However, oocyte and embryo mitochondria were sufficiently active at basal level to reduce the icO_2 by up to 29% in comparison to the minimum represented by antimycin treated icO_2 .

Oxygen consumption is often used as a representative proxy of overall metabolism, and is widely reported to increase progressively throughout preimplantation development^{18,51}. By the blastocyst stage, a significant increase in metabolic activity reportedly results in 2–4 times more oxygen being consumed than in cleavage-stage embryos as measured by pyrene fluorescence of small groups of 2–32 embryos^{51,52}, extracellular flux analysis of small groups of 6 embryos²⁵, or single-embryo nanorespirometry¹⁵. This increase is most likely due to the requirement for sufficient oxygen to power blastocoel formation. In the present study, blastocyst icO_2 was higher than that of EC embryos and mature oocytes.

Additionally, further analysis of MM2-labelled blastocysts suggested that the majority of the oxygen was present in the TE, with significantly lower icO_2 in the ICM (Fig. 4). If icO_2 was taken purely as an index of oxygen consumption, then this would suggest that (1) blastocysts were less metabolically active than other stages and (2) the ICM was more metabolically active than the TE. However, previous reports have established that this is not the case¹⁷. In fact, ICM mitochondria tend to be fewer and less active, retaining their globular, immature physiology until post-implantation, while TE mitochondria tend to begin maturation during blastocyst development^{17,26}. The present data therefore paints a more complex picture than can be easily explained by reports of oxygen consumption. It is tempting to speculate that oxygen may diffuse rapidly into the TE cells lining the outermost layer of the blastocyst, leading to a higher icO_2 . However rapid oxygen consumption by the highly metabolically

active TE mitochondria could leave a reduced amount to diffuse to the ICM. Interestingly, Byatt-Smith et al. predicted that oxygen could diffuse to the centre of smaller embryos (e.g. murine), but cannot diffuse to the centre of the larger bovine embryos⁵³. While this is speculative, future study may reveal the dynamics of oxygen diffusion and metabolism in blastocysts. Nevertheless, the present data suggests that the MM2 probe is sensitive to differences in oxygen concentration in different regions of the embryo.

Comparison of blastocyst icO_2 and total cell count or cell allocation ratio did not reveal any significant correlations (Fig. 5A,B). This data suggests that blastocyst icO_2 was not significantly dependent on the total number of cells or allocation to TE or ICM. Cell allocation ratios were assayed using the method of Thouas et al.⁵⁴. This method is widely used due to its relative ease and accessibility, and care was taken to expose blastocysts to the PI stain in Triton X for the minimum time to lyse the zona and stain the outermost cells only. However future use of an immunofluorescence approach using antibody markers of the ICM-specific Sox2 and TE-specific Cdx2 could improve specificity and reduce subjectivity^{55–57}. Kuno et al. recently reported a positive correlation between chimeric mouse blastocyst OCR measured using a chip-based electrochemical method and increasing total cell count measured by this immunocytochemical approach²³.

In analyses of oocytes and embryos, the copy number of mitochondrial genomes is often used as an index of the number of individual mitochondria. This is due to reports that, on average, individual oocyte mitochondria each have around 1.3 copies of mtDNA^{35,58,59}. In the present study, mtDNA copy number varied greatly within oocyte and embryo developmental stages in the range $0.9\text{--}4 \times 10^6$ copies (Fig. 6A). This range is comparable to published reports, for example Cotterill et al.³³ reported 0.74×10^6 copies per ovine MII oocyte, and aligned with a putative 1×10^5 mtDNA copy number threshold for oocyte competence. In the current study no significant differences in mtDNA copy number were observed between oocyte and embryo stages (Fig. 6B). This contrasts to previous reports, in which mtDNA copy number increased significantly during oocyte maturation⁶⁰ and preimplantation embryo development⁶¹. No correlation was observed between basal icO_2 and mtDNA count between or within stages ($p=0.14$, Fig. 6A,B). This agrees with a recent report from Kuno et al., in which chimeric mouse blastocyst OCR did not correlate with mtDNA copy number²³. In this study, mtDNA copy number was not correlated to icO_2 in the samples measured. However, changes in oxidative activity of mitochondria during preimplantation development may also be dependent on changes in mitochondrial maturation and embryo morphology.

This study reports that the commercially available MM2 probe is non-toxic and effective in measuring icO_2 in mammalian oocytes and preimplantation embryos, including comparison of distinct regions. This method has many potential applications in investigating mitochondrial activity in reproductive tissues, particularly when used in combination with established techniques.

Materials and methods

All chemicals were obtained from Sigma-Aldrich (Dorset, UK) unless otherwise indicated.

Bovine tissue acquisition. Ethical approval for animal work was not required for this study as all bovine tissue was derived from non-pregnant animals slaughtered at a local abattoir (John Penny and sons, Leeds, UK) for commercial food production purposes only. The authors were not involved in this process. Bovine reproductive tracts were collected from the abattoir and transported to the laboratory within 2 h of slaughter. The ovaries were dissected from the tracts and live oocytes were aspirated as described below. Bovine embryos were produced *in vitro* from these oocytes using cryopreserved spermatozoa based on established protocols^{51,62,63}. *In vitro* preimplantation embryo development was maintained to the blastocyst stage for a maximum of 8 days as described below and no animal or embryo transfer studies were conducted.

***In vitro* production of bovine embryos.** Ovaries were dissected from tracts in the laboratory and washed in pH 7.45 Phosphate Buffer Saline (PBS) comprising 1.058 mM Potassium Phosphate Monobasic, 155.17 mM Sodium Chloride and 2.97 mM Sodium Phosphate Dibasic supplemented with Penicillin, Streptomycin and Amphotericin B (Fungizone) at 39 °C.

Follicular fluid containing live oocytes was aspirated from antral follicles of 2- < 10 mm diameter by aspiration with a pre-warmed syringe fitted with an 18-gauge needle containing a small amount of HEPES-buffered holding medium. Holding medium was Medium-199 supplemented with 4 mM NaHCO_3 , 21.1 mM HEPES, 0.02 mg/ml Heparin, 2 mg/ml Fatty Acid-Free Bovine Serum Albumin (BSA-FAF, A6003) and 100 IU/ml Penicillin/Streptomycin⁶². Cumulus-Oocyte Complexes (COCs) were matured in groups of 50 for 18–24 h in 500 μl *In-Vitro* Maturation (IVM) Medium at 39 °C under humidified 5% CO_2 in air according to the protocols reported by Hemmings et al.⁶². Serum-free IVM medium consisted of bicarbonate-buffered α -Minimum Essential Medium supplemented with 2 mM glutamine, 0.47 mM pyruvate, 5 $\mu\text{g/ml}$ Sodium Selenite, 10 ng/ml Insulin, 10 ng/ml Long-R3 IGF-1, 0.0006 IU/ml bovine FSH, 0.0003 IU/ml bovine LH, 1 mg/ml BSA-FAF and 100 IU/ml 100 IU/ml Penicillin/Streptomycin.

Oxygen metabolism was quantified in oocytes at 2 discrete stages of meiotic maturity. A subset of cumulus enclosed immature oocytes were analysed immediately following follicle aspiration. Oocytes were denuded of cumulus cells by repeat pipetting through 170 μm and 140 μm EZ-grip embryo handling pipette tips (RI Systems) in 80 IU/ml bovine hyaluronidase in HEPES-buffered MEM at 37 °C. Mature oocytes were collected following 24 h of IVM. Cumulus cells were removed as described above and meiotic progression to MII was confirmed by detection of first polar body extrusion using light microscopy.

In Vitro Fertilisation (IVF) was carried out using frozen-thawed spermatozoa from a bull of proven fertility (Genus, Cheshire, UK). Sperm were centrifuged on a discontinuous Percoll gradient (45:90%) for 30 min at 760 Relative Centrifugal Force (RCF) to select motile sperm. Sperm wash medium was HEPES-Tyrodé's

Albumin Lactate Pyruvate (H-TALP) medium comprising 114 mM NaCl, 3.19 mM KCl, 0.45 mM NaH₂PO₄, 2 mM NaHCO₃, 0.26 mM pyruvate, 7.5 mM HEPES, 2.06 mM CaCl₂, 0.49 mM MgCl₂, 9.96 mM lactate, 4 mg/ml BSA-FAF and 0.05 mg/ml gentamycin. Selected sperm were washed in H-TALP at 330 × g for a further 5 min before co-incubation with mature COCs in Fertilisation-TALP (F-TALP) at a concentration of 1 × 10⁶ ml⁻¹ for 18 h at 39 °C and 5% CO₂ in humidified air. F-TALP was 114 mM NaCl, 3.19 mM KCl, 0.45 mM NaH₂PO₄, 25 mM NaHCO₃, 0.26 mM pyruvate, 2.06 mM CaCl₂, 0.49 mM MgCl₂, 9.96 mM lactate, 10 µg/ml heparin, 2 µM penicillamine, 1 µM hypotaurine, 4 mg/ml BSA-FAF and 0.05 mg/ml gentamycin.

Putative zygotes were collected from IVF plates in 500 µl HEPES-buffered Synthetic Oviduct Fluid (H-SOF) then denuded of remaining cumulus cells by vortexing for 2 min. H-SOF comprised 111 mM NaCl, 7.16 mM KCl, 1.19 mM NaH₂PO₄, 5 mM NaHCO₃, 0.33 mM pyruvate, 1.5 mM glucose, 33.2 mM lactate, 20 mM HEPES, 1.71 mM CaCl₂, 4.9 mM MgCl₂, 9.96 mM lactate, 4 mg/ml BSA-FAF and 100 IU/ml Penicillin/Streptomycin. Putative zygotes were then selected in H-SOF and transferred to SOF culture medium supplemented with amino acids and BSA-FAF (SOFaaBSA) in groups of 40 using a glass pipette. SOFaaBSA comprised 111 mM NaCl, 7.16 mM KCl, 1.19 mM NaH₂PO₄, 5 mM NaHCO₃, 0.33 mM pyruvate, 1.5 mM glucose, 33.2 mM lactate, 0.1 mM glutamine, 1.71 mM CaCl₂, 4.9 mM MgCl₂, 9.96 mM lactate, 1 × BME Essential and Non-Essential Amino acids 8 mg/ml BSA-FAF and 100 IU/ml Penicillin/Streptomycin. The zygotes were washed twice in SOFaaBSA before moving to 20 µl pre-equilibrated microdrops under mineral oil for culture in groups of 20 in hydrophobic IVF culture dishes. Embryo culture dishes were incubated at 39 °C under 5% CO₂, 5% O₂, 90% N₂ in humidified air in a Cook MINC mini-incubator for up to 8 days. Mean oocyte maturation rates were 76.2 ± 2.5% and blastocyst development rates were 25.35 ± 9.01%.

Labelling oocytes and embryos with the MM2 probe. MM2 probe labelling and imaging methods were adapted from those of Kondrashina et al.³⁸ and Prill et al.⁴². Pilot experiments confirmed that 24 h incubation in bicarbonate-buffered media led to increased signal intensity in the blue and red channels as well as increased sensitivity in the red channel to changes in oxygen concentration due to mitochondrial inhibition (A). Subsequent experiments showed that extending the incubation time to 72 h had no effect on intensity or signal ratio. Samples were labelled with 5 µg/ml MM2 in 500 µl IVM for oocytes and 5 µg/ml MM2 in 20 µl SOFaaBSA for embryos. Fluorescence values were converted to oxygen concentration in µmol/l using a calibration curve (Fig. 1). Calibration was achieved by plotting signal intensity ratios of fixed oocytes or embryos in 21% oxygen and 0% oxygen environments as described by Prill et al.⁴². Samples were fixed overnight in 2% glutaraldehyde, 2% formaldehyde in PBS to ablate oxygen consuming activity but maintain 3D structure. These samples were imaged in 10mM sodium dithionite in PBS to remove all O₂ but otherwise labelled as normal with 5 µg/ml MM2 and imaged as detailed above. Samples for normoxia were fixed to ablate oxygen-consuming activity before rehydration with probe solution to ensure maximal O₂ content with zero consumption. Therefore, these were fixed and dehydrated with ethanol before rehydrating with fresh media containing 5 µg/ml MM2 (Fig. 1).

Multiphoton imaging was performed on a Zeiss LSM 710 microscope with Chameleon multiphoton laser. The parfocal distance of the upright multiphoton microscope was insufficient to support use of standard live-cell imaging chambers. Therefore, oocyte and embryo samples were mounted on glass slides, in 5 µl drops of appropriate HEPES-buffered media (e.g. HM for oocytes and HSOF for embryos). Media drops were flanked by 2 layers of labelling tape and overlaid with a glass coverslip. This allowed removal and replacement of the media drop with fresh media supplemented with the required inhibitor for each stage of the experiment.

Profiling of mitochondrial activity throughout oocyte and embryo development. icO₂ under basal, maximal and non-mitochondrial conditions were measured sequentially in the same samples as follows. Respiratory chain inhibitors were dissolved in molecular biology grade ethanol, a vehicle which does not significantly change preimplantation embryo oxygen consumption⁶⁴, to investigate how aspects of the bioenergetic profile change throughout preimplantation development. Following measurement of basal oxygen levels, media on the imaging slide was replaced with 5 µl pre-warmed HEPES-buffered media supplemented with 5 µg/ml MM2 and 10 µM Carbonyl Cyanide-P-Trifluoromethoxyphenylhydrazone (FCCP). Samples were incubated for 30 min to allow equilibration of oxygen concentration. This increased OCR to the maximum possible (the maximal respiratory rate). The difference between maximal and basal OCR is the *spare respiratory capacity* and indicative of how close the tissue is to its bioenergetic limit^{14,30}. This was followed by treatment with antimycin, an inhibitor of complex III. This effect was immediate, as, once mitochondrial OCR is blocked, oxygen diffuses back into the tissue instantly. Samples were incubated for 5 min to ensure oxygen diffusion had re-equilibrated and for parity between experiments.

Image analysis. Multiphoton images were examined in ImageJ™. A circular region of interest was selected around each oocyte or embryo sample and mean signal intensity was measured in the blue (reference) and red (oxygen-sensitive) channels. An MM2 probe signal ratio was calculated by dividing red (oxygen-sensitive) signal by total (blue + red) MM2 signal. This was converted to units of oxygen concentration (µmol/l) by referencing to a 2-point calibration curve (Fig. 1C). All subsequent analyses were completed in GraphPad Prism™ 8. Data was analysed for normality by the D'Agostino-Pearson test. Parametric data was analysed by ANOVA with post-hoc Bonferroni test for significant differences between groups, while non-parametric data was tested by Friedman's test (for paired data) or Kruskal-Wallis test (for unpaired data) with post-hoc Dunn's test for significant differences between groups. Data comparisons with $p < 0.05$ were regarded as significantly different.

Mitochondrial DNA copy number. A subset of samples was flash frozen in liquid nitrogen in 10 µl PBS for mitochondrial DNA (mtDNA) copy number analysis by quantitative real-time Polymerase Chain Reaction

(qPCR). A synthesised plasmid was used as a DNA control spike. The method was adapted from those of Cotterill et al.³³ and Hashimoto et al.⁶⁵. Primers were designed for the mitochondrially-encoded gene COI (cytochrome c oxidase subunit 1) with a PCR product measuring 129 bases. The primer sequences were: 5' CGTTGTCGC ACATTTCCACTA 3'(forward), 5' GCGAAGTGGATTTTGGCTCAT 3' (reverse). A spike plasmid (pGEM T-easy vector, Promega, Madison USA) was used as an internal control with forward primer 5'CTAGTGATT GTGCGGGAGAGA3' and reverse 5'CTTTGAAATTGGCTGGATTGTG3' and a 152 bp product. The spike was used at a 1/1000 dilution to achieve a similar number of copies in the same order of magnitude as the COI samples through a series of preliminary validation experiments. mtDNA was extracted from a pool of 10 oocytes to identify expected concentrations in these initial validations. Briefly, 10 µl of 2X lysis buffer (2X PCR buffer, 1% Triton X-100 and 200 ng/ml proteinase K) was added to the 10 µl sample for a total sample volume of 20 µl. Cell lysis was performed in a PCR thermal cycler by heating to 55 °C for 30 min then 95 °C 5 min. 2 µl of lysate was used as template in a 25 µl reaction with real-time qPCR master mix comprising: 9.25 µl DNase/RNase free water, (1.25 µl primers (of 10 µM working stocks) and 2.5 µl SYBR Green Master Mix (Applied Biosystems, CA, USA). The qPCR conditions were: Denaturing at 95 °C for 10 min (1 cycle), Amplification at 95 °C for 30 s, 60 °C for 30 s, 72 °C for 1 min (35 cycles), Melt curve at 95 °C, Cooling at 37 °C for 5 min and then maintained at 4 °C until sample collection. qPCR was carried out and data were analysed using a Roche LightCycler 480 and software. The standard curve used to quantify each experimental sample included serial dilutions in the range 10×10^3 to 10×10^8 copies or 0.1–0.000001 ng/ml of the purified PCR product. Mean extraction efficiency calculated as an index of expected vs extracted spike copy number was 82%.

Cell allocation ratios. Total cell counts and cell allocation ratios were calculated by the method of Thouas et al.⁵⁴. Briefly, blastocysts were first transferred to propidium iodide (100 µg/ml) and 0.001% Triton X-100 in PBS for 30 s to stain TE cells. To prevent labelling of the ICM, blastocysts were immediately washed 3 × in PBS, before transferring to 25 µg/ml Hoechst 3342 in ethanol to label all cell nuclei. Total cell number was counted at 460 nm 3 times and TE cell count was recorded 3 times at 560 nm using a Zeiss Axioscope A1 epifluorescence microscope (Cambridge, UK). The mean of 3 counts were used to calculate the percentage TE out of total cells. The number of ICM cells was calculated by subtracting TE cells from the total Hoechst-stained cells.

Statistical analyses. Data were tested for normality using the D'Agostino-Pearson test. Parametric data were compared using Student's t-test or ANOVA with post-hoc Tukey test dependant on the number of groups for comparison. Non-parametric data were compared using Mann–Whitney U test or Kruskal Wallis with post-hoc Dunn's test. All analyses were performed in GraphPad Prism 6.

The data underlying this article will be shared on reasonable request to the corresponding author.

Received: 1 June 2021; Accepted: 24 August 2021

Published online: 28 October 2021

References

1. Thouas, G. A., Trounson, A. O., Wolvetang, E. J. & Jones, G. M. Mitochondrial dysfunction in mouse oocytes results in preimplantation embryo arrest in vitro. *Biol. Reprod.* **71**, 1936–1942 (2004).
2. Kasapoğlu, I. & Seli, E. Mitochondrial dysfunction and ovarian aging. *Endocrinology* <https://doi.org/10.1210/endoqr/bqaa001> (2020).
3. Nagai, S. *et al.* Correlation of abnormal mitochondrial distribution in mouse oocytes with reduced developmental competence. *Tohoku J. Exp. Med.* **210**, 137–144 (2006).
4. Wang, Y. M., Qiu, M. Y., Liu, Q., Tang, H. & Gu, H. F. Critical role of dysfunctional mitochondria and defective mitophagy in autism spectrum disorders. *Brain Res. Bull.* **168**, 138–145 (2021).
5. Rojas-Charry, L., Nardi, L., Methner, A. & Schmeisser, M. J. Abnormalities of synaptic mitochondria in autism spectrum disorder and related neurodevelopmental disorders. *J. Mol. Med.* <https://doi.org/10.1007/s00109-020-02018-2> (2020).
6. Nunnari, J. & Suomalainen, A. Mitochondria: in sickness and in health. *Cell* **148**, 1145–1159 (2012).
7. Beal, M. F. Energetics in the pathogenesis of neurodegenerative diseases. *Trends Neurosci.* **23**, 298–304 (2000).
8. Coskun, P. *et al.* A mitochondrial etiology of alzheimer and parkinson disease. *Biochim Biophys Acta* **1820**, 553–564 (2012).
9. Fragouli, E. *et al.* Altered levels of mitochondrial DNA are associated with female age, aneuploidy, and provide an independent measure of embryonic implantation potential. *PLoS Genet.* **11**, e1005241 (2015).
10. Berg, J. M., Tymoczko, J. L. & Stryer, L. *Biochemistry* (W H Freeman, 2002).
11. Leese, H. J. Metabolism of the preimplantation embryo: 40 years on. *Reproduction* **143**, 417–427 (2012).
12. Leese, H. J. & Barton, A. M. Pyruvate and glucose uptake by mouse ova and preimplantation embryos. *Reproduction* **72**, 9–13 (1984).
13. Leese, H. J. What does an embryo need?. *Hum. Fertil.* **6**, 180–185 (2003).
14. Birket, M. J. *et al.* A reduction in ATP demand and mitochondrial activity with neural differentiation of human embryonic stem cells. *J. Cell Sci.* **124**, 348–358 (2011).
15. Lopes, A. S. *et al.* Respiration rates of individual bovine in vitro-produced embryos measured with a novel, non-invasive and highly sensitive microsensor system. *Reproduction (Cambridge, England)* **130**, 669–679 (2005).
16. Trimarchi, J. R., Liu, L., Porterfield, D. M., Smith, P. J. S. & Keefe, D. L. A non-invasive method for measuring preimplantation embryo physiology. *Zygote (Cambridge, England)* **8**, 15–24 (2000).
17. Houghton, F. D. Energy metabolism of the inner cell mass and trophectoderm of the mouse blastocyst. *Differ. Res. Biol. Divers.* **74**, 11–18 (2006).
18. Lopes, A. S., Lane, M. & Thompson, J. G. Oxygen consumption and ROS production are increased at the time of fertilization and cell cleavage in bovine zygotes. *Hum. Reprod.* **25**, 2762–2773 (2010).
19. Shiku, H. *et al.* Oxygen consumption of single bovine embryos probed by scanning electrochemical microscopy. *Anal. Chem.* **73**, 3751–3758 (2001).
20. Shiku, H. *et al.* Respiration activity of single bovine embryos entrapped in a cone-shaped microwell monitored by scanning electrochemical microscopy. *Anal. Chim. Acta* **522**, 51–58 (2004).

21. Hiramoto, K. *et al.* Development of oxygen consumption analysis with an on-chip electrochemical device and simulation. *Anal. Chem.* **89**, 10303–10310 (2017).
22. Kurosawa, H. *et al.* Development of a new clinically applicable device for embryo evaluation which measures embryo oxygen consumption. *Hum. Reprod.* **31**, 2321–2330 (2016).
23. Kuno, T. *et al.* A preclinical evaluation towards the clinical application of oxygen consumption measurement by CERMs by a mouse chimera model. *Int. J. Mol. Sci.* **20**, 5650 (2019).
24. Obeidat, Y. M. *et al.* Design of a multi-sensor platform for integrating extracellular acidification rate with multi-metabolite flux measurement for small biological samples. *Biosens. Bioelectron.* <https://doi.org/10.1016/j.bios.2019.02.069> (2019).
25. Muller, B. *et al.* Application of extracellular flux analysis for determining mitochondrial function in mammalian oocytes and early embryos. *Sci. Rep.* **9**, 1–14 (2019).
26. van Blerkom, J. Mitochondrial function in the human oocyte and embryo and their role in developmental competence. *Mitochondrion* **11**, 797–813 (2011).
27. Brand, M. D. Uncoupling to survive? The role of mitochondrial inefficiency in ageing. *Exp. Gerontol.* **35**, 811–820 (2000).
28. Buttgerit, F. & Brand, M. D. A hierarchy of ATP-consuming processes in mammalian cells. *Biochem. J.* **312**(1), 163–167 (1995).
29. Lewis, A. N., Hinrichs, K., Leese, H. J. & Argo, C. M. Glucose concentration during equine. *Reproduction* **1160**, 227–237 (2020).
30. Brand, M. D. & Nicholls, D. G. Assessing mitochondrial dysfunction in cells. *Biochem. J.* **435**, 297–312 (2011).
31. Zeng, H. T. *et al.* Low mitochondrial DNA and ATP contents contribute to the absence of birefringent spindle imaged with PolScope in *in vitro* matured human oocytes. *Hum. Reprod.* **22**, 1681–1686 (2007).
32. Sturmey, R. G., O’Toole, P. J. & Leese, H. J. Fluorescence resonance energy transfer analysis of mitochondrial:lipid association in the porcine oocyte. *Reproduction (Cambridge, England)* **132**, 829–837 (2006).
33. Cotterill, M. *et al.* The activity and copy number of mitochondrial DNA in ovine oocytes throughout oogenesis *in vivo* and during oocyte maturation *in vitro*. *Mol. Hum. Reprod.* **19**, 444–450 (2013).
34. Spikings, E. C., Alderson, J., St. John, J. C. & St. John, J. C. Regulated mitochondrial DNA replication during oocyte maturation is essential for successful porcine embryonic development. *Biol. Reprod.* **76**, 327–335 (2007).
35. Cummins, J. M. The role of maternal mitochondria during oogenesis, fertilization and embryogenesis. *Reprod. Biomed.* **4**, 176–182 (2002).
36. van Blerkom, J. Domains of high-polarized and low-polarized mitochondria may occur in mouse and human oocytes and early embryos. *Hum. Reprod.* **17**, 393–406 (2002).
37. Larsson, N.-G. *et al.* Mitochondrial transcription factor A is necessary for mtDNA maintenance and embryogenesis in mice. *Nat. Genet.* **18**, 231–236 (1998).
38. Kondrashina, A. V. *et al.* A phosphorescent nanoparticle-based probe for sensing and imaging of (intra)cellular oxygen in multiple detection modalities. *Adv. Funct. Mater.* **22**, 4931–4939 (2012).
39. Fercher, A., Borisov, S. M., Zhdanov, A. V., Klimant, I. & Papkovsky, D. Intracellular O₂ sensing probe based on cell-penetrating phosphorescent nanoparticles. *ACS Nano* **5**, 5499–5508 (2011).
40. Dmitriev, R. I., Zhdanov, A. V., Jasioneck, G. & Papkovsky, D. Assessment of cellular oxygen gradients with a panel of phosphorescent oxygen-sensitive probes. *Anal. Chem.* **84**, 2930–2938 (2012).
41. Dmitriev, R. I. & Papkovsky, D. Optical probes and techniques for O₂ measurement in live cells and tissue. *Cell. Mol. Life Sc. CMLS* **69**, 2025–2039 (2012).
42. Prill, S., Andersson, A., Papkovsky, D. & Schmäzlin, E. Intracellular O₂ measurements: fluorescent microscopy with nanosensors. *GIT Lab. J.* **1**, 28–29 (2014).
43. Guarino, R. D. *et al.* Method for determining oxygen consumption rates of static cultures from microplate measurements of pericellular dissolved oxygen concentration. *Biotechnol. Bioeng.* **86**, 775–787 (2004).
44. Fraker, C. *et al.* The use of the BD oxygen biosensor system to assess isolated human islets of langerhans: oxygen consumption as a potential measure of islet potency. *Cell Transplant.* **15**, 745–758 (2006).
45. Lavrentieva, A., Majore, I., Kasper, C. & Hass, R. Effects of hypoxic culture conditions on umbilical cord-derived human mesenchymal stem cells. *Cell Commun. Signal.* **8**, 1–9 (2010).
46. Ferreira, F. *et al.* Real-time physiological measurements of oxygen using a non-invasive self-referencing optical fiber microsensors. *Nat. Protoc.* **15**, 207–235 (2020).
47. Lopes, A. S., Greve, T. & Callesen, H. Quantification of embryo quality by respirometry. *Theriogenology* <https://doi.org/10.1016/j.theriogenology.2006.09.026> (2007).
48. Lopes, A. S. *et al.* Investigation of respiration of individual bovine embryos produced *in vivo* and *in vitro* and correlation with viability following transfer. *Hum. Reprod.* <https://doi.org/10.1093/humrep/del404> (2007).
49. Dmitriev, R. I. *et al.* Imaging oxygen in neural cell and tissue models by means of anionic cell-permeable phosphorescent nanoparticles. *Cell. Mol. Life Sci.* **72**, 367–381 (2015).
50. Dmitriev, R. I., Zhdanov, A. V., Nolan, Y. M. & Papkovsky, D. Imaging of neurosphere oxygenation with phosphorescent probes. *Biomaterials* **34**, 9307–9317 (2013).
51. Thompson, J. G., Partridge, R. J., Houghton, F. D., Cox, C. I. & Leese, H. J. Oxygen uptake and carbohydrate metabolism by *in vitro* derived bovine embryos. *Reproduction* **106**, 299–306 (1996).
52. Houghton, F. D., Thompson, J. G., Kennedy, C. J. & Leese, H. J. Oxygen consumption and energy metabolism of the early mouse embryo. *Mol. Reprod. Dev.* **44**, 476–485 (1996).
53. Byatt-Smith, J. G., Leese, H. J. & Gosden, R. G. An investigation by mathematical modelling of whether mouse and human pre-implantation embryos in static culture can satisfy their demands for oxygen by diffusion. *Hum. Reprod.* **6**, 52–57 (1991).
54. Thouas, G. A., Korfiatis, N. A., French, A. J., Jones, G. M. & Trounson, A. O. Simplified technique for differential staining of inner cell mass and trophoctoderm cells of mouse and bovine blastocysts. *Reprod. Biomed. Online* **3**, 25–29 (2001).
55. Liu, S. *et al.* Sox2 is the faithful marker for pluripotency in pig: evidence from embryonic studies. *Dev. Dyn.* **244**, 619–627 (2015).
56. Yoon, J. D. *et al.* GDF8 enhances SOX2 expression and blastocyst total cell number in porcine IVF embryo development. *Theriogenology* **129**, 70–76 (2019).
57. Kwak, S. S., Jeung, S. H., Biswas, D., Jeon, Y. B. & Hyun, S. H. Effects of porcine granulocyte-macrophage colony-stimulating factor on porcine *in vitro*-fertilized embryos. *Theriogenology* **77**, 1186–1197 (2012).
58. Pikó, L. & Taylor, K. D. Amounts of mitochondrial DNA and abundance of some mitochondrial gene transcripts in early mouse embryos. *Dev. Biol.* **123**, 364–374 (1987).
59. Pikó, L. & Matsumoto, L. Number of mitochondria and some properties of mitochondrial DNA in the mouse egg. *Dev. Biol.* **49**, 1–10 (1976).
60. Iwata, H. *et al.* Effect of maternal age on mitochondrial DNA copy number, ATP content and IVF outcome of bovine oocytes. *Reprod. Fertil. Dev.* **23**, 424 (2011).
61. McConnell, J. M. & Petrie, L. Mitochondrial DNA turnover occurs during preimplantation development and can be modulated by environmental factors. *Reprod. Biomed.* **9**, 418–424 (2004).
62. Hemmings, K. E., Leese, H. J. & Picton, H. M. Amino acid turnover by bovine oocytes provides an index of oocyte developmental competence *in vitro*. *Biol. Reprod.* **86**, 165 (2012).
63. Gordon, I. *Laboratory Production of Cattle Embryos*. Biotechnology in agriculture series, vol 27. 2nd ed. CABI (2003).
64. McKeegan, P. J. *Metabolic Regulation During Early Embryo Development* (2015).

65. Hashimoto, S. *et al.* Quantitative and qualitative changes of mitochondria in human preimplantation embryos. *J. Assist. Reprod. Genetics* <https://doi.org/10.1007/s10815-017-0886-6> (2017).
66. Donnay, I. & Leese, H. J. Embryo metabolism during the expansion of the bovine blastocyst. *Mol. Reprod. Dev.* **53**, 171–178 (1999).
67. Sturme, R. G. & Leese, H. J. Energy metabolism in pig oocytes and early embryos. *Reproduction* **126**, 197–204 (2003).

Acknowledgements

The authors would like to thank John Penny and sons, Leeds UK for tissue supply. Many thanks to Professor Dmitri Papkovsky for the kind gift of MM2 probe samples. Many thanks to Professor David Beech for use of the multiphoton microscope, David Myers for training and support, the British Heart Foundation for funding the multiphoton microscope, and the Wellcome Trust for subsidising its use for pilot studies. This work was supported by an Eric Reid Fund for Methodology award to PJM by the Biochemical Society. LJW was supported by a Society for Reproduction and Fertility Summer Studentship. SB and AW contributed to this study as part of their MSc Clinical Embryology and Assisted Reproduction Technologies Dissertation Projects. PJM was funded as a post-doctoral researcher by the Medical Research Council, UK. Grant Ref: MR/K020501-1 awarded to HMP.

Author contributions

Conceived and designed the experiments: P.J.M., G.B., A.W., S.B., L.J.W., K.G., J.L., H.M.P. Performed the experiments: P.J.M., G.B., A.W., S.B., L.J.W., K.G. Analysed the data: P.J.M., G.B., A.W., S.B., K.G., J.L. Contributed to the writing of the manuscript: P.J.M., S.B., A.W., K.G., H.M.P. Critically revised the manuscript and approved the final draft: P.J.M., G.B., A.W., S.B., L.J.W., K.G., J.L., H.M.P.

Competing interests

The authors declare no competing interests.

Additional information

Correspondence and requests for materials should be addressed to P.J.M.

Reprints and permissions information is available at www.nature.com/reprints.

Publisher's note Springer Nature remains neutral with regard to jurisdictional claims in published maps and institutional affiliations.



Open Access This article is licensed under a Creative Commons Attribution 4.0 International License, which permits use, sharing, adaptation, distribution and reproduction in any medium or format, as long as you give appropriate credit to the original author(s) and the source, provide a link to the Creative Commons licence, and indicate if changes were made. The images or other third party material in this article are included in the article's Creative Commons licence, unless indicated otherwise in a credit line to the material. If material is not included in the article's Creative Commons licence and your intended use is not permitted by statutory regulation or exceeds the permitted use, you will need to obtain permission directly from the copyright holder. To view a copy of this licence, visit <http://creativecommons.org/licenses/by/4.0/>.

© The Author(s) 2021